Insight into the Role of Gut Microbiota in Duchenne Muscular Dystrophy

Maxence Jollet, Mahendra Mariadassou, Olivier Rué, Laurence Pessemesse, Vincent Ollendorff, Sofiane Ramdani, Barbara Vernus, Anne Bonnieu, Christelle Bertrand-Gaday, Benedicte Goustard, et al.

The American Journal of Pathology, Vol. ■, No. ■, ■ 2023

The American Journal of PATHOLOGY
ajp.amjpathol.org

Insight into the Role of Gut Microbiota in Duchenne Muscular Dystrophy

An Age-Related Study in mdx Mice

Maxence Jollet,* Mahendra Mariadassou,[†‡] Olivier Rué,[†‡] Laurence Pessemesse,* Vincent Ollendorff,* Sofiane Ramdani,[§] Barbara Vernus,* Anne Bonnieu,* Christelle Bertrand-Gaday,* Bénédicte Goustard,* and Christelle Koechlin-Ramonatxo*

From the DMEM, Université de Montpellier, INRAE, Montpellier; Université Paris-Saclay,[†] INRAE, BioinfOmics, MIGALE Bioinformatics Facility, Jouy-en-Josas; Université Paris-Saclay,[‡] INRAE, MaIAGE, Jouy-en-Josas; and LIRM,[§] Université de Montpellier, CNRS, Montpellier, France*

Accepted for publication October 31, 2023.

Address correspondence to Maxence Jollet, Ph.D., French National Institute for Food, Agriculture, and Environment, University of Montpellier, 2 Place Pierre Viala, 34070 Montpellier, France; or Christelle Koechlin-Ramonatxo, Ph.D., French National Institute for Food, Agriculture, and Environment, University of Montpellier, 2 Place Pierre Viala, Bat 22, 34070 Montpellier, France. E-mail: christelle.ramonatxo@umontpellier.fr or maxence.jollet@ki.se.

Dystrophin deficiency alters the sarcolemma structure, leading to muscle dystrophy, muscle disuse, and ultimately death. Beyond limb muscle deficits, patients with Duchenne muscular dystrophy have numerous transit disorders. Many studies have highlighted the strong relationship between gut microbiota and skeletal muscle. The aims of this study were: i) to characterize the gut microbiota composition over time up to 1 year in dystrophin-deficient *mdx* mice, and ii) to analyze the intestine structure and function and expression of genes linked to bacterial-derived metabolites in ileum, blood, and tibial anterior and soleus muscles to study interorgan interactions. *Mdx* mice displayed a significant reduction in the overall number of different operational taxonomic units and their abundance (α-diversity). *Mdx* genotype predicted 20% of β-diversity divergence, with a large taxonomic modification of the four phyla (Actinobacteria, Proteobacteria, Tenericutes, and Deferribacteres) and the included genera. Interestingly, intestinal motility and gene expressions of tight junction and *Ffar2* receptor were down-regulated in the ileum of the *mdx* genotype. Concomitantly, inflammation related to gut microbiota was revealed by an up-regulation of circulating inflammatory markers (tumor necrosis factor, IL-6, and monocyte chemoattractant protein-1) and muscle inflammation *Tlr4/Myd88* pathway (Toll-like receptor 4, which recognizes pathogen-associated molecular patterns, known as the bacterial metabolites receptor). Finally, in *mdx* mice, adiponectin was reduced in blood and its receptor modulated in muscles. This study highlights a specific gut microbiota composition and highlights interorgan interactions in *mdx* physiopathology with gut microbiota as the potential central metabolic organ. *(Am J Pathol 2023, ■: 1–16; https://doi.org/10.1016/j.ajpath.2023.10.010)*

Duchenne muscular dystrophy (DMD) is a progressive wasting disease of skeletal and cardiac muscles, and one of the most common recessive inherited genetic diseases (yearly incidence, 1:3500-1:5000 boys). In DMD, mutations in the *DMD* gene affect the proper production of the membrane-associated dystrophin protein, leading to weakening of the muscle cell membrane to mechanical stress during the contraction/relaxation cycles that promotes microlesions. These lesions can initially be associated with muscle pseudo-hypertrophy, especially in postural muscles (eg, triceps surae muscles), highlighting the muscle fiber regenerative capacities. The endless cycles of muscle necrosis and repair lead to fibrosis and progressive muscle weakness. Proximal skeletal muscles are the most affected: first, the locomotor muscles, then the trunk muscle, and finally the respiratory muscles and the heart, leading to quadriplegia and cardio-respiratory difficulties. Moreover, many secondary pathophysiological processes exacerbate muscle pathology in DMD: immunologic and inflammatory processes,[1,2] altered calcium homeostasis,[3,4] oxidative

Supported by a recurrent annual operating budget from the French National Research Institute for Agriculture, Food, and Environment and the University of Montpellier without specific grants.

https://doi.org/10.1016/j.ajpath.2023.10.010

stress,[5] and apoptosis and defective autophagy,[6] as well as declines in mitochondrial number and function.[7,8]

Actual therapies can be divided in two categories: primary therapy (to restore or partially restore functional dystrophin protein) and other therapeutic approaches (to improve muscle function and quality in patients with DMD). The current primary therapies are exon skipping, stop codon readthrough, gene addition, genome editing, and myoblast transplantation.[9] In addition, many therapeutic avenues are being evaluated to improve muscle condition by targeting fibrosis, growth and regeneration processes, calcium homeostasis, or mitochondria biogenesis.[9] In these therapeutic approaches, such as identification of small molecules[10] or exercise,[11] an new strategy is emerging: nutraceuticals.[12] Thanks to the current standards of care, many patients with DMD can now expect to live into their fourth decade of life. However, in the absence of a curative treatment, prevention of secondary processes that exacerbate DMD pathophysiology and offer improvement in the patients' quality of life are a priority. In this context, it is important to better understand the processes associated with DMD development and the links between the affected organs, including the possible crosstalk between gut microbiota and skeletal muscle.

The term "gut microbiota" describes the 10^{14} bacteria housed in the digestive tract and classified in different species, families, and phyla. This bacterial community plays an important role in the host metabolism and health. Due to the functional crosstalk with other organs (eg, brain, heart, liver, adipose tissue), perturbations of the gut microbiota composition and function (ie, dysbiosis) have been associated with many diseases, such as brain disorders (eg, depression, autism, Alzheimer disease) and metabolic disorders (eg, obesity, type 2 diabetes, insulin resistance). Moreover, several studies have shown the implication of the intestinal microbiota in antitumor treatment effectiveness[13–15] and in cachexia (ie, the cancer-associated loss of skeletal muscle and adipose tissue). Indeed, Bindels et al[16] found that the gut microbiota was depleted in a leukemic and cachexic mouse model. Interestingly, when the gut microbiota was normalized by oral supplementation of probiotics, the concentration in muscle of inflammation markers [IL-6, IL-4, monocyte chemoattractant protein-1 (MCP-1), and granulocyte colony-stimulating factor], autophagy markers (LC3 and cathepsin L), and proteolysis markers (atrogin1 and MAFbx) decreased. The probiotic treatment also prevented skeletal muscle inflammation and atrophy. Since this first study suggesting a gut microbiota–skeletal muscle axis, accumulating evidence has highlighted the potential influence of gut microbiota on the skeletal muscle phenotype. Muscle mass is reduced in germ-free mice that lack microbiota compared with control mice.[17,18] Our laboratory showed that gut bacteria are necessary to optimize skeletal muscle function. Indeed, depletion of gut bacteria by treatment with broad-spectrum antibiotics led to a decrease in skeletal muscle endurance and to an alteration in glucose homeostasis, as indicated by the decreased expression of short-chain fatty acid chain (SCFA) and glucose transporters in the ileum, and reduced glycogen content in muscle. This phenotype was normalized after natural reseeding.[19] Similarly, Yan et al[20] observed that after transfer of gut microbiota from obese or lean pigs to germ-free mice, mice replicated the donor's skeletal muscle fiber profile.

Different pathways might be involved in the gut microbiota–skeletal muscle axis. Several circulating mediators, such as pro-inflammatory cytokines, SCFA, and branched-chain amino acids, in relation with the gut microbiota composition, have recognized effects on skeletal muscle. For example, microbiota-derived SCFAs (eg, acetate, butyrate, propionate) are produced during a gut microbial fermentation process and could drive skeletal muscle toward an oxidative metabolism. Similarly, in mice fed a high-fat diet, butyrate supplementation is associated with improved insulin sensitivity, increased *peroxisome proliferator–activated receptor-γ coactivator-1α* and AMP-activated protein kinase activity (regulation of energy metabolism), and a higher proportion of type 1 fibers in skeletal muscle.[21] Moreover, the muscle-specific SCFA receptors FFAR3 and FFAR2 promote insulin sensitivity and modulate glucose uptake. These findings suggest that gut microbiota composition/function in DMD might be altered, with possible effects on the host's health and myopathy. However, very few exploratory data are available on intestinal smooth muscle in DMD, although dystrophin is expressed in smooth muscle,[22,23] and intestinal function is altered in patients with DMD. Moreover, gastrointestinal alterations, including aerophagia, gastroesophageal reflux, and constipation (affecting nearly 70% of patients for this last item), have been documented in these patients.[24]

Gut bacterial community alteration in DMD could be potentiated by the fact that this chronic disease is associated with conditions that promote intestinal dysbiosis in other pathologic contexts. For instance, a sedentary lifestyle has deleterious effects on microbial composition,[25] and treatments prescribed to patients with DMD, particularly antibiotics to treat respiratory infections,[26] deplete the intestinal microbiota.[13] Therefore, to exclude these extrinsic factors, gut microbiota composition could be studied in *mdx* mice, an animal model of DMD. Some studies reported that, similar to patients with DMD, *mdx* mice exhibit increased intestinal peristalsis[27] and reduced fecal excretion,[28–30] particularly due to an alteration of the migrant motor complex responsible for mobility in the interdigestive period.[31]

The aims of the current study were: i) to characterize the gut microbiota composition in *mdx* mice and its changes during disease development by comparing the α- and β-diversity of taxonomic profiles and gut microbiota abundance (16S rRNA gene metagenomic analysis) in *mdx* mice and control littermates at 8 weeks, 12 weeks, 6 months, and 1 year of age, ii) to measure plasma biomarkers that could mediate the skeletal muscle–gut microbiota crosstalk, and

FLA 5.6.0 DTD ■ AJPA3994_proof ■ 24 November 2023 ■ 1:30 am ■ EO: AJPA-D-22-

iii) to investigate the intestine structure and contractile properties, as well as the expression in the ileum and muscle, of genes linked to bacterial-derived metabolites to identify microbiota−muscle interactions in the *mdx* phenotype.

Materials and Methods

Animal Care

Male *mdx* mice (C57BL10SnSc-DMD^{mdx}/J) and wild-type mice [B10: wild-type C57BL10SnSc raised in the laboratory's animal facility (F2 generation)] were used at different ages (8 weeks, 12 weeks, 6 months, and 1 year) ($n = 10$ per group per age). Mice were housed in ventilated cages (20°C to 22°C, 12:12 hour light−dark cycle) with food and water *ad libitum*. The diet (3395 kcal/kg) was standardized and identical for all groups (SAFE A03; SAFE, Augy, France). It included 69.2% cereals, 20.2% vegetal protein, 6.0% animal protein, and 4.6% of a mineral and vitamin cocktail. The following is a general description of the macronutrient composition: 61.3% protein carbohydrates, 25.2% protein, and 13.5% lipids. The study experimental protocols complied with the European directives on animal experimentation (86/609/EEC) and were approved by the French National Ethics Committee (APAFIS#19430-2019022513523628v2).

Stool Collection

Feces were collected directly from the anus of the mice at 8 weeks, 12 weeks, 6 months, and 1 year of age. Samples were then immediately frozen in liquid nitrogen before storage at −80°C.

Euthanasia and Sample Collection

Mice were fasted for 12 hours and then euthanized by intraperitoneal injection of ketamine (100 mg/kg) and xylazine (20 mg/kg). Blood was collected via inferior vena cava sampling and centrifuged at 2500 × *g* for 15 minutes; the plasma supernatant was snap-frozen and stored at −80°C. Intestinal tissue samples (duodenum, jejunum, ileum, and colon), cecum content, and soleus and tibial anterior (TA) samples were collected, weighed, and immediately frozen in liquid nitrogen and stored at −80°C. Second TA samples were collected and placed directly in isopentane cooled in liquid nitrogen and stored at −80°C. Both extensor digitorum longus (EDL) muscles were carefully removed and tendons tied with braided surgical silk for future *ex vivo* contractility.

TA Staining by Immunohistochemistry

Serial transverse sections (10 μm thick) from liquid nitrogen−cooled isopentane TA muscle samples embedded in optimal cutting temperature medium were obtained using a cryostat at −25°C and mounted on glass microscope slides. Sections were then washed in phosphate-buffered saline, blocked, and permeabilized with 0.1% Triton X-100 and 10% horse serum. Staining was performed with anti-laminin (L9393; 1/200; MilliporeSigma, Burlington, MA), anti-dystrophin (ab15277; 1/200; Abcam, Cambridge, United Kingdom), and Hoechst. This was followed by secondary antibody incubation with 546 donkey anti-rabbit (Fluoroprobes, Interchim; 1/500) for anti-laminin and Alexa 488 goat anti-rabbit (1/1000; Thermo Fisher Scientific, Waltham, MA) for anti-dystrophin. Whole histologic sections were imaged with an automated imaging device (MRI-INM; Axioscan; Zeiss, Oberkochen, Germany) and analyzed with ImageJ software version 1.53p (NIH, Bethesda, MD; http://imagej.nih.gov/ij).

Ex Vivo Assessment of Contractility in EDL

Muscle contractile properties were assessed in *ex vivo* conditions as previously described.[32] This technique allows evaluation of the intrinsic muscle contractile properties. After 15 minutes' equilibration in the Krebs solution bath continually bubbled with 95% oxygen to 5% carbon dioxide (pH 7.4) and thermostatically maintained at 37°C, EDL samples were connected to a force transducer/length servomotor system (model 305B; Cambridge Instruments, Aurora Scientific Inc., Aurora, ON, Canada) and were stimulated along their entire length with platinum wire electrodes. The optimum muscle length (ie, the muscle length producing maximal twitch tension) was determined. All subsequent measurements were made at the optimum muscle length. The isometric tetanic tension was determined (701B Stimulator, Aurora Scientific Inc.) using stimulation trains of 500 milliseconds, with pulse duration of 0.5 millisecond at different frequencies, from 1 to 150 Hz. Stimulus trains were separated by a 1-minute interval. The maximum isometric tetanic tension was determined from the plateau of the frequency-tension curve. Three minutes after the tension-frequency determination, the resistance to fatigue was evaluated by using a low-frequency fatigue protocol of 50 Hz trains of 700 milliseconds delivered every 2 seconds for 5 minutes. The muscle fatigue index was defined as the time taken to produce a 50% reduction from the initial maximum power output. After all measurements, EDL samples were removed from the bath, trimmed of the connective tissue, blotted dry, and weighed. For each animal, the second EDL was placed in oxygenized Krebs solution throughout the procedure and was used in case of emergency.

Detection and Quantification of Plasma Proteins

One-quarter of the diluted plasma samples were analyzed by using the Meso Scale Discovery U-PLEX Metabolic Group 1 (ms) 11-Plex assays. The antibody set contains

FLA 5.6.0 DTD ■ AJPA3994_proof ■ 24 November 2023 ■ 1:30 am ■ EO: AJPA-D-22-

biotinylated capture antibodies and corresponding detection antibodies for 11 proteins: IL-1b, IL-4, Il-6, tumor necrosis factor, MCP-1, ghrelin (active and total), glucagon-like peptide-1 (active and total), leptin, and peptide YY (total). Assays were performed following manufacturer's instructions using Meso Scale Discovery 96-well, 10-spot plates and recommended diluents, with all plasma samples being vortexed thoroughly before use. For experimental measurements with below detection limits, concentrations were considered as "0." Levels of circulating adiponectin were measured by using ELISA. Adiponectin doses were determined by using commercial ELISA kits (#DY1065; R&D Systems, Minneapolis, MN) according to the manufacturer's instructions.

Ex Vivo Jejunum Basal Contractile Function

Jejunum basal contractile properties were assessed *ex vivo* at 1 year of age. Specifically, 1 cm of the first part of the jejunum was connected to a force transducer/length servomotor system (model 305B; Cambridge Instruments, Aurora Scientific Inc.). The optimum smooth muscle length (ie, the muscle length producing maximal twitch tension) was determined. All subsequent measurements were made at optimum smooth muscle length. After 15 minutes' equilibration in Krebs solution continually bubbled with 95% oxygen to 5% carbon dioxide (pH 7.4) and thermostatically maintained at 37°C, the basal peristalsis was recorded at 200 Hz for 15 minutes. This method is adapted from Alves et al.[33] To determine the period of peristalsis, the signal obtained with DMC version 3.500 software (Aurora Scientific Inc.) was extracted and imported to MATLAB 1.8.0_202 (MathWorks, Portola Valley, CA), in which a fast Fourier transform was used to convert the signal to a frequency domain. The peak frequency was then obtained as the frequency corresponding to the peak of the power spectrum. The period P was then estimated as the inverse of the peak frequency.

Histologic Analyses of the Small Intestine

The small intestine was removed, divided into two parts with the mucosal layer outward using a long wooden stick and immersed in a solution of 4% paraformaldehyde in phosphate buffer (0.1 mol/L, pH 7.4) for 4 hours at room temperature.[34] They were then rinsed in phosphate buffer and immersed in 20% sucrose in phosphate buffer (0.1 M, pH 7.4) for 24 hours at 4°C. Two parts of the intestine were opened longitudinally and coiled with the mucosal layer outward using a wooden stick, embedded in optimal cutting temperature medium, and frozen in isopentane cooled in liquid nitrogen. Swiss Rolls of intestine were cut in longitudinal sections into serial 10 μm thick slices and stained with hematoxylin and eosin and Alcian blue (stain goblets cells) for histologic analysis. Goblet cell density was determined by counting blue-stained cells per *millimeter* of intestine. Whole histologic sections were imaged with a digital slide scanner (MRI-INM platform; Nano-Zoomer 2.0-HT; Hamamatsu, Montpellier, France). The analysis was performed on NDP.view 2 software (Hamamatsu). Five fields of the same surface (7 mm^2) were captured, and all cells marked were counted and analyzed with ImageJ software version 1.53p

For structural analysis, Swiss Rolls of intestine were cut in longitudinal sections into serial 10 μm thick slices and stained with anti-laminin (L9393; 1/200; MilliporeSigma), anti-dystrophin (ab15277; 1/200; Abcam), and Hoechst. This was followed by secondary antibody incubation with 546 donkey anti-rabbit (Fluoroprobes; Interchim; 1/500) for anti-laminin and Alexa 488 goat anti-rabbit (1/1000; Thermo Fisher Scientific) for anti-dystrophin. The images were acquired with an automated imaging device (Axioscan; Zeiss, Oberkochen, Germany) provided by the facility imaging MRI-INM (Institute of Neuroscience, Montpellier, France).

mRNA Expression Analysis by Quantitative RT-PCR

Total RNA was isolated from ileum, TA, and soleus samples using TRIzol (15596-018, Invitrogen, Carlsbad, CA). RNA concentration was determined by spectrophotometric analysis (BioDrop DUO; BioDrop, Cambridge, UK), and purity was checked by calculating the OD_{260nm}/OD_{280nm} absorption ratio (>1.8). RNA quality was verified by using 1% agarose gel electrophoresis. Reverse transcription was performed with 2 μg of total RNA and the high-capacity cDNA Reverse Transcription Kit (catalog no. 4368813; Applied Biosystems) according to the manufacturer's instructions. One-tenth of the obtained cDNA was used in each PCR assay. real-time quantitative PCR analysis was performed using a Step One Plus detection system (AB Applied Biosystems) with 10 μL of Mastermix (PowerUp SYBR Green Master Mix, Scientific A25742; Thermo Fisher Scientific), 10 nmol/L of forward and reverse primers, 5 μL of diluted cDNA template, and water to a final volume of 15 μL. Forward and reverse primers are listed in Table 1.

All PCR assays were performed in duplicate using the following cycling parameters: 50°C for 2 minutes, then 95°C for 2 minutes followed by 40 cycles of 95°C for 3 seconds and 60°C for 30 seconds. Relative mRNA levels were normalized to the levels of the housekeeping genes *Arp*, *Tubulin-α* for ileum samples, and *Arp* and *Rps9* for TA and soleus samples. Results are expressed using the comparative cycle threshold method to generate $\Delta\Delta C_T$ values with template dilutions ranging from 10^1 to 10^6 copies. The PCR overall efficiency (E) was calculated from the standard curve slopes according to the equation $E = [10^{(-1/slope)}] - 1$, and this value was >95% for all assays. The relative abundance of each sample was normalized according to the equation: Relative Quantity $= 2^{-\Delta\Delta C_T}$.

FLA 5.6.0 DTD ■ AJPA3994_proof ■ 24 November 2023 ■ 1:30 am ■ EO: AJPA-D-22-

Table 1 Primers Used for qPCR in Ileum, Soleus, and TA

Function	Sample	Gene name	Forward primer	Reverse primer
Housekeeping genes	Ileum, Soleus, TA	*Arp*	5′-TCCCACCTTGTCTCCAGTCT-3′	5′-ACTGGTCTAGGACCCGAGAAG-3′
	Ileum	*Tubulin-α*	5′-GTGGCCACGAGCATAGTTATT-3′	5′-CTGGAACCCACGGTCATC-3′
	Soleus, TA	*Rps9*	5′-ATCCGCCAACGTCACATTA-3′	5′-TCTTCAGTCGCCTGGAC-3′
Tight junction proteins and gut permeability	Ileum	*Zo-1*	5′-AAATCATCCGACTCCTCGTC-3′	5′-CAGTTGGCTCCAACAAGGTAA-3′
	Ileum	*Zo-2*	5′-CAGGCATGGAGGAGGTGA-3′	5′-CACGGCAATTCCAAATCC-3′
	Ileum	*Cldn5*	5′-ACGGGAGGAGCGCTTTAC-3′	5′-GTTGGCGAACCAGCAGAG-3′
	Ileum	*Ocln*	5′-TCCTCCTGGCTCAGTTGAA-3′	5′-CCAGGCTCCCAAGATAAGC-3′
	Ileum	*Jam1*	5′-AGAACAAAGAAAGGGACTGCAC-3′	5′-ACCAGGAACGACGAGGTCT-3′
SCFA receptors	Ileum	*Ffar1*	5′-AGGCGCTCTCCTCACACTC-3′	5′-CTAGCCACATTGGAGGCATTA-3′
	Ileum, Soleus	*Ffar3*	5′-CATCCTCCTGCCTGTACGAC-3′	5′-ATACACAGGGGCACCATGA-3′
	Ileum, Soleus	*Ffar2*	5′-TGCTCTGAAGAAGCCAATCA-3′	5′-TTCTCCTCTGGTCCAGTGCT-3′
LCFA receptor	Ileum	*Ffar4*	5′-TTGGTGTTGAGCGTCGTG-3′	5′-CCAGCAGTGAGACGACAAAG-3′
BCAA receptor	Soleus	*Bcat2*	5′-TGGAGACACTTTGAACACATGAGC-3′	5′-TCTTTTGGACCCACATAGAAGC-3′
Lipid metabolism	Ileum, Soleus	*Angptl4*	5′-GGGACCTTAACTGTGCCAAG-3′	5′-GAATGGCTACAGGTACCAAACC-3′
Glucose transporter	Soleus	*Slc2a4*	5′-GACGGACACTCCATCTGTTG-3′	5′-GCCACGATGGAGACATAGC-3′
Inflammation	Ileum, Soleus	*Myd88*	5′-GCCTTGTTAGACCGTGAGGAT-3′	5′-CTAAGTATTTCTGGCAGTCCTCCT-3′
	Ileum, Soleus	*Tlr4*	5′-GGACTCTGATCATGGCACTG-3′	5′-CTGATCCATGCATTGGTAGGT-3′
	Ileum, Soleus	*Nfkb1*	5′-TGAGGACGGGGTATGCAC-3′	5′-TCACATGAAGTATTCCCAGGTTT-3′
	Soleus	*Trif*	5′-CAGCTCAAGACCCCTACAGC-3′	5′-CTCCCACACAGCCTCGTC-3′
Adiponectin receptors	Soleus, TA	*Adipor1*	5′-GTTTGCCACTCCCAAGCA-3′	5′-ACACCACTCAAGCCAAGTCC-3′
	Soleus, TA	*Adipor2*	5′-TCTCAGTGGGACATGTTTGC-3′	5′-AGGCCTAAGCCCACGAAC-3′

Adipor1, adiponectin receptor 1; *Adipor2*, adiponectin receptor 2; *Angptl4*, fasting-induced adipose factor; *Arp*, acidic ribosomal phosphoprotein; BCAA, branched-chain amino acids; *Bcat2*, branched-chain-amino-acid aminotransferase; *Cldn5*, claudin-5; *Ffar1*, Free-fatty acid receptor 1; *Ffar2*, Free-fatty acid receptor 2; *Ffar3*, Free-fatty acid receptor 3; *Ffar4*, Free-fatty acid receptor 4; *Jam1*, junctional adhesion molecule A; LCFA, long-chain fatty acids; *Myd88*, myeloid differentiation primary response 88; *Nfkb1*, nuclear factor kappa B; *Ocln*, occludin; qPCR, real-time quantitative PCR; *Rps9*, 40S ribosomal protein S9; SCFA, short-chain fatty acids; *Slc2a4*, glucose transporter 4; TA, tibial anterior; *Tlr4*, Toll-like receptor 4; *Trif*, TIR-domain-containing adapter molecule 1; *Zo-1*, zonula occludens 1; *Zo-2*, zonula occludens 2.

DNA Extraction from Feces

Total cell DNA was extracted from 0.1 g of animal fecal material using the G'NOME Kit (BIO 10; MP Biomedicals, La Jolla, CA) with modifications.[35] Fecal samples were homogenized in the supplied cell suspension solution. Cell lysis/denaturing solution was added, and samples were incubated at 55°C for 2 hours. To improve cell lysis, 0.1-mm diameter silica beads (750 μL) were added, and samples were mixed at the maximum speed in a Fast-Prep bench homogenizer (MP Biomedicals) for 4 minutes. Polyvinylpolypyrrolidone (15 mg) was added to ensure removal of polyphenol contamination that could inhibit the real-time quantitative PCR assays. Samples were vortexed and centrifuged at 20,000 × *g* for 3 minutes, and supernatants were recovered. The remaining pellets were washed with 400 μL of TENP [50 mmol/L Tris (pH 8), 20 mmol/L EDTA (pH 8), 100 mmol/L NaCl, 1% Polyvinylpolypyrrolidone] and centrifuged at 20,000 × *g* for 3 minutes. The washing step was repeated once, and the resulting supernatants pooled. Nucleic acids were precipitated by addition of one volume of isopropanol, incubation at −20°C for 20 minutes, and centrifugation at 20,000 × *g* for 10 minutes. Pellets were resuspended in 400 μL of distilled water plus 100 μL of salt-out mixture and incubated at 4°C for 10 minutes. Samples were spun at maximum speed for 10 minutes, and DNA-containing supernatants were transferred to clean 1.5-mL microcentrifuge tubes. DNA was precipitated with two volumes of 100% ethanol at room temperature for 5 minutes, followed by centrifugation at 16,000 × *g* for 5 minutes. DNA was resuspended in 150 μL of TE buffer and stored at −20°C.

Evaluation of Microbiota Composition by Sequencing

The V3-V4 region of the 16SrRNA genes was amplified using the bacterial primers 343F (5′-CTTTCCCTAC ACGACGCTCTTCCGATCTACGGRAGGCAGCAG-3′) and 784R (5′-GGAGTTCAGACGTGTGCTCTTCCGAT CTTACCAGGGTATCTAATCCT-3′) modified to add adaptors during the second PCR amplification. PCR assays were performed by using the MolTaq 16S DNA polymerase and the corresponding master mix (Molzym GmbH & Co. KG, Bremen, Germany). The PCR mix contained 10 ng of DNA, 1 μL of dNTPs (10 mmol/L), 1.25 μL each of forward and reverse primer (20 μM), and 0.5 μL of Taq polymerase in a total volume of 50 μL. The cycling program was as follows: 94°C for 3 minutes, followed by 40 cycles at 94°C for 15 seconds, 60°C for 30 seconds, 72°C

FLA 5.6.0 DTD ■ AJPA3994_proof ■ 24 November 2023 ■ 1:30 am ■ EO: AJPA-D-22-

for 60 seconds, and a final extension at 72°C for 5 minutes. Sequencing was performed by using MiSeq technology (Illumina) at the Genopole Toulouse Midi-Pyrenees genomic facility (Toulouse, France).

Metagenomic Analysis

Sequencing data were demultiplexed at the Genopole Toulouse Midi-Pyrenees platform. Version 3.2.3 was used to produce abundance tables of operational taxonomic units (OTUs) and their taxonomic affiliation[36] following author guidelines.[37] The most abundant sequences of each OTU were then matched with blastn to the Silva version 132 database.[38] Abundance tables and taxonomy files were imported into RStudio (version 1.2.1335), and phyloseq 1.28.0,[39] ggplot2 3.4.0,[40] and custom scripts were used for data analysis. Samples were rarefied to even sampling depths before computing within-sample compositional diversities (Observed richness, Chao1, Shannon, and InvSimpson) and between-samples compositional diversity (UniFrac). Principal coordinates analysis was also performed on dissimilarity matrices to obtain a two-dimensional representation of the samples. Alpha diversity data were analyzed by using repeated measures analysis of variance. Permutational multivariate analysis of variance tests were performed on UniFrac matrices using 9999 random permutations and a significance level of 0.01. The relative abundances of phyla were compared by using repeated measures analysis of variance and GraphPad Prism version 10.0.0 for Windows (GraphPad Software, La Jolla, CA). As published by Segata et al,[41] the linear discriminant effect size (LEfSe) method was performed by combining the Kruskal-Wallis test or Wilcoxon rank-sum test with the linear discriminant analysis scores to estimate the effect size of differentially abundant features with biologic consistency and statistical significance (the α value was set at 0.05, and the linear discriminant analysis score threshold for discriminative features was >2.0)[41] (The Huttenhower Lab, *http://huttenhower.sph.harvard.edu/galaxy*, last accessed December 5, 2022).

Q19 The data sets analyzed in this article are publicly available [*https://data.inrae.fr/data set.xhtml?persistentId=doi:10.57745/ZSX5M4*; last accessed October 5, 2023 (login required)].

Statistical Analysis

All data are presented as means ± SEM. Statistical significance was checked by using two-way analysis of variance to compare the *mdx* and B10 groups at different time points; when not applicable, a *t*-test was used. For all statistical analyses, the significance level was set at 0.05. Data were analyzed by using GraphPad Prism version 10.0.0 for Windows.

Results

Reduced Gut Microbiota α- and β-Diversities in *mdx* Genotype

Comparison of the Observed, Chao1, and InvSimpson indices obtained at different ages showed that α-diversity varied between genotypes. Specifically, the Observed ($P < 0.01$) and Chao1 ($P < 0.05$) indices were significantly reduced, whereas the InvSimpson index was increased, in *mdx* mice compared with wild-type B10 littermates (Figure 1A). The Shannon index was comparable between [F1] genotypes (Figure 1A). The graphical representation of β-diversity using principal coordinates analysis plots for the UniFrac distances showed a strong and significant effect of the genotype ($P < 0.001$) (Figure 1B). Separate analysis at each time point confirms that the separation of the genotype is significant at all time points ($P < 0.001$). The ordination plot shows that the first axis of the principal coordinates analysis corresponds to the genotype and accounts for almost 20% of the diversity ($P < 0.0001$) (Figure 1B).

Specific Taxonomic Modification of Main Phyla and Included Genera in *mdx* Genotype

Comparison of the abundance of the six main phyla during the first year of life revealed significant differences in gut microbiota composition in *mdx* and B10 mice. The abundance of Actinobacteria, Proteobacteria, and Tenericutes was significantly increased in *mdx* mice compared with B10 mice (Figure 2). Moreover, the Deferribacteres phylum was [F2] only present in *mdx* mice (all ages tested) (Figure 2).

Analysis of the differential abundances using LEfSe highlighted 30 up-regulated OTUs (including eight unknown genera and species) in the gut microbiota of *mdx* mice compared with B10 mice. Conversely, nine OTUs (including eight unknown genera and species) were characteristic of B10 mice based on their linear discriminant analysis score compared with *mdx* mice (Figure 3A). *Bacteroidaceae*, [F3] *Bacteroides*, *Alistipes*, *Rikenellaceae*, *Rhodospirillales*, *Rhodospirillaceae*, *Deferribacterales*, *Deferribacteraceae*, and *Deferribacteres* were overexpressed by at least 3.6-fold in *mdx* mice. Conversely, the Lachnospiraceae NK4A136 group and Bacteroidales S24_7 group were decreased by almost 4.8-fold in B10 mice.

The cladogram representation of the LEfSe results according to the taxonomic rank (Figure 3B) allowed easy identification of the taxonomic branches (from phyla to OTUs) that were modified in *mdx* mice, as well as the extent of the modification. The abundance of the phylum Deferribacteres was increased in *mdx* mice, as was the class Deferribacteres, the order Deferribacterales, the family *Deferribacteraceae*, and the genus *Mucispirillum*. Similarly, two other main continuous taxonomic changes were identified in *mdx* mice: the phylum Proteobacteria, then the class (Alphaproteobacteria), order (Rhodospirillales), family

FLA 5.6.0 DTD ■ AJPA3994_proof ■ 24 November 2023 ■ 1:30 am ■ EO: AJPA-D-22-

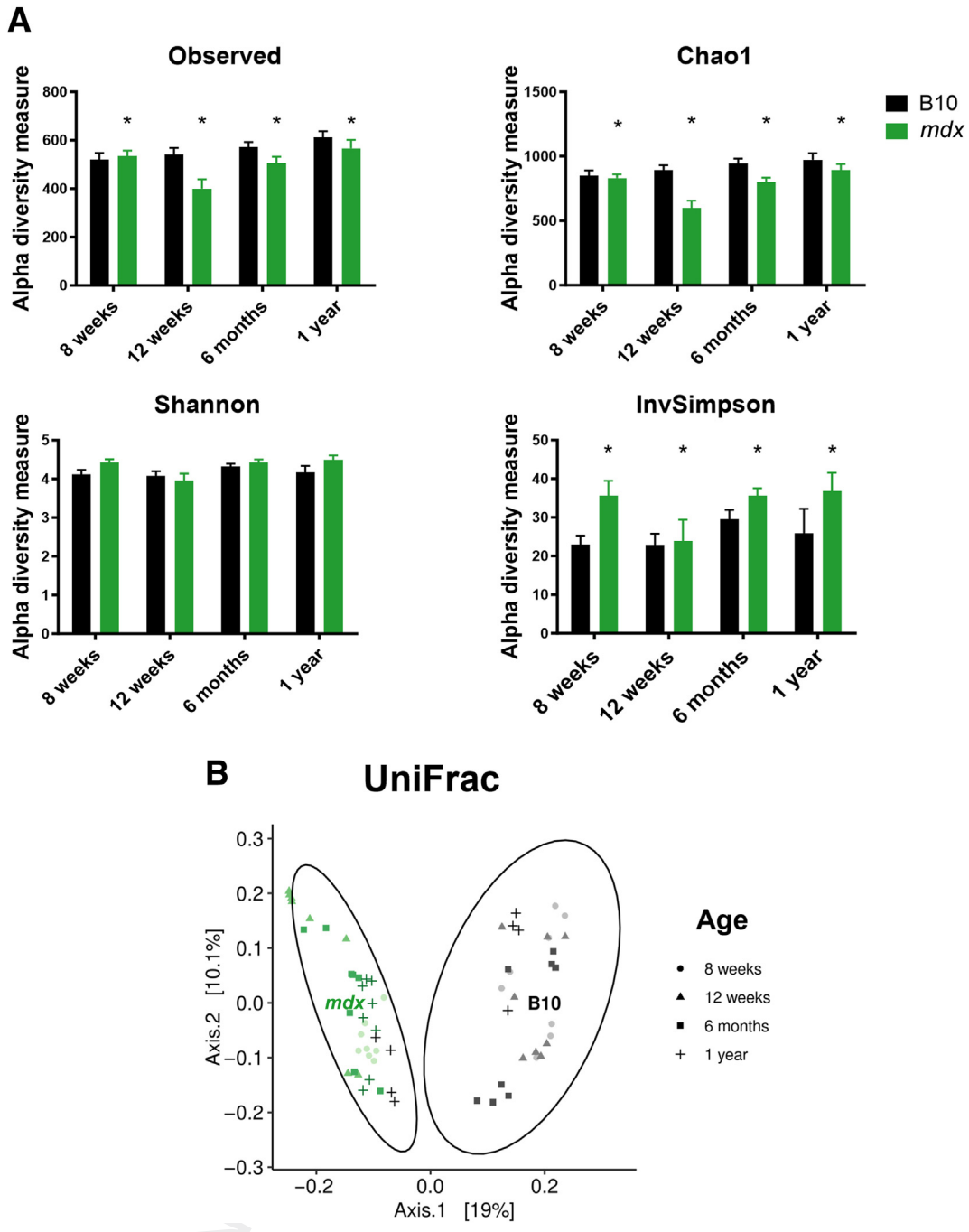

Figure 1 Dystrophin deficiency is associated with gut microbiota α- and β-diversity altered. **A:** α-Diversity indices in *mdx* (C57BL10SnSc-DMD^{mdx}/J) mice and B10 (wild-type C57BL10SnSc) mice from 8 weeks to 1 year of age. **B:** Principal coordinates analysis plots of β-diversity between genotypes using the UniFrac distances. $N = 10$ per group per age. Green: *mdx* mice; Black: B10 mice. Point: 8 weeks; triangle: 12 weeks; square: 6 months; cross: 1 year. *$P < 0.05$ versus B10 mice.

(*Rhodospirillaceae*), and genus (unknown species); and the phylum Actinobacteria, then the class (Coriobacteriia), order (Coriobacteriales), family (*Coriobacteriaceae*), and genus (*Enterorhabdus*) (Figure 3B). For other phyla, some taxonomic ranks were altered; for instance, the prevalence of *Bacteriodes* and *Bacteriodaceae* belonging to the Bacteriodetes phylum was increased. Moreover, the Lachnospiraceae NK4A136 group from the Firmicutes phylum was reduced in B10 mice. No impact of dystrophin deficiency in the phylum Tenericutes was observed, however.

Low-Grade Circulating Inflammation and Reduced Adipokines Levels in *mdx* Genotype

Plasma biomarker analysis highlighted a low-grade inflammation in *mdx* mice characterized by higher levels

FLA 5.6.0 DTD ■ AJPA3994_proof ■ 24 November 2023 ■ 1:30 am ■ EO: AJPA-D-22-

print & web 4C/FPO

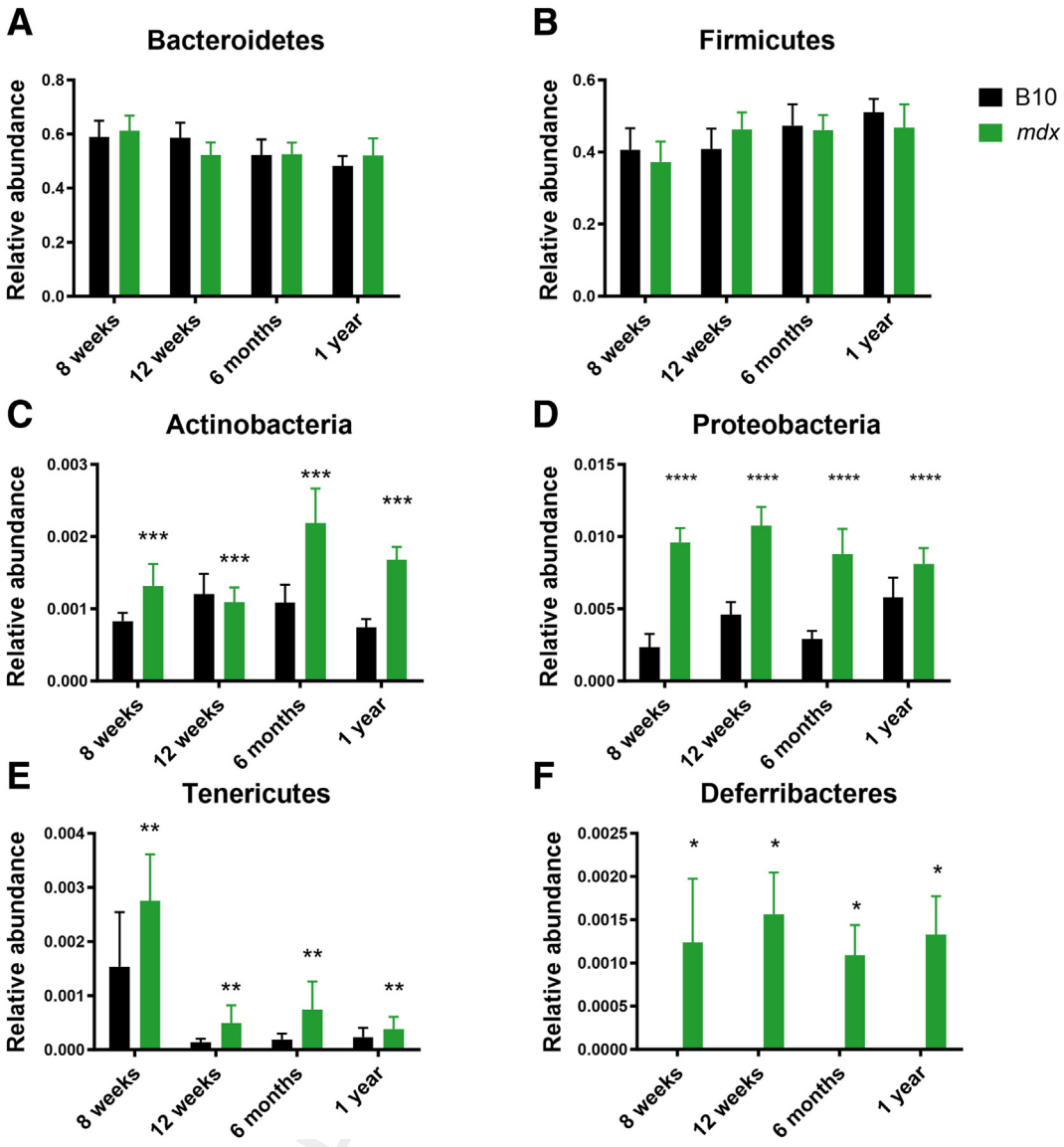

Figure 2 Four major gut microbiota phyla are increased in *mdx* (C57BL10SnSc-DMD^{mdx}/J) mice. Relative abundance of Bacteriodetes phylum (**A**), Firmicutes phylum (**B**), Actinobacteria phylum (**C**), Proteobacteria phylum (**D**), Tenericutes phylum (**E**), and Deferribacteres phylum (**F**) at 8 weeks, 12 weeks, 6 months, and 1 year of age. $n = 10$ per group per age. $^{*}P < 0.05$, $^{**}P < 0.01$, $^{***}P < 0.001$, $^{****}P < 0.0001$ versus B10 (wild-type C57BL10SnSc) mice.

of IL-6 (Figure 4A), tumor necrosis factor (Figure 4B), and MCP-1 (Figure 4C) compared with B10 mice. IL-1β involved in the inflammatory process was not modulated (Supplemental Table S1), and IL-4 was undetectable in both groups.

In addition, our data revealed a strong down-regulation of circulating adipokines such as adiponectin (Figure 4D) and leptin (Figure 4E) in *mdx* mice compared with their B10 littermates. Interestingly, as shown in Table 2, adiponectin and leptin explain 10% and 11.9%, respectively, of the gut microbiota signature of dystrophin-deficient mice.

The entero-endocrine hormone ghrelin differs between groups, with a normalization with age of circulating level in *mdx* mice compared with B10 mice (Supplemental Table S1). Nevertheless, glucagon-like peptide-1 and peptide YY measurements did not reveal differences between groups (Supplemental Table S1).

Slowed Down Gut Peristalsis in *mdx* Genotype, Not Likely Linked with the Dystrophin Protein Deficiency

In *mdx* mice, the limited amount of dystrophin protein synthesis is characterized by altered structure and function of skeletal muscle (Supplemental Figure S1A). Indeed, even with hypertrophy during the first 6 months of life (Supplemental Figure S1, B–D), hindlimb muscles revealed a force weakness from 8-week–old worthening with aging (Supplemental Figure S1E).

Because gut microbiota is involved in intestinal smooth muscle motility, intestine morphology and function were

FLA 5.6.0 DTD ■ AJPA3994_proof ■ 24 November 2023 ■ 1:30 am ■ EO: AJPA-D-22-

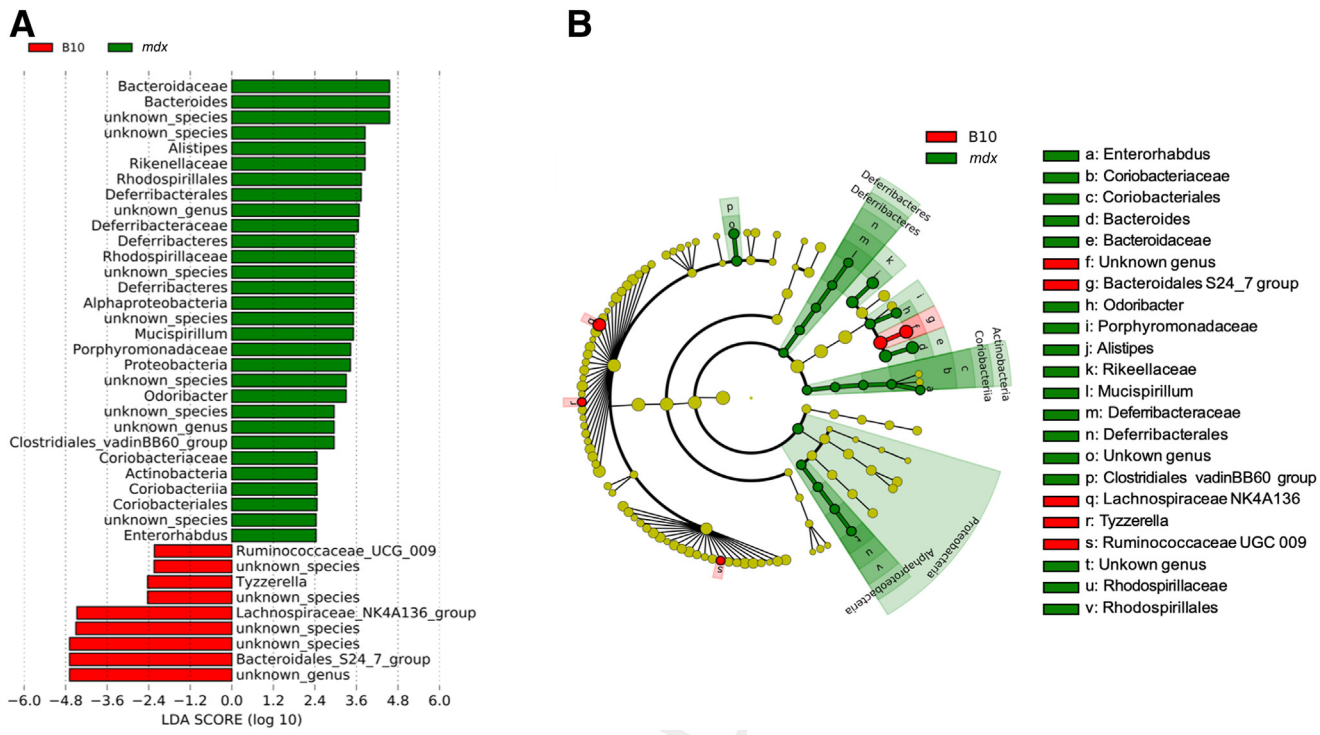

print & web 4C/FPO

Figure 3 Operational taxonomic unit abundances in *mdx* (C57BL10SnSc-DMD^{mdx}/J) mice and B10 (wild-type C57BL10SnSc) mice. **A:** Linear discriminant analysis (LDA) effect size for the two genotype (all ages). The figure shows the microbial taxa, the abundance of which was significantly different between *mdx* (green) and B10 (red) mice. **B:** Cladogram representation of the microbiota composition in *mdx* and B10 mice. The cladogram plot shows the differences in the relative abundances of taxa at six levels between *mdx* and B10 mice. All plots were generated by using the online Galaxy Huttenhower Lab server. Each cycle represents a stratification from phylum (inner) up to genera (outer). $n = 10$ per group per age.

investigated. Dystrophin staining by immunofluorescence revealed an absence of dystrophin in the intestine independently of the phenotype (Figure 5A). In addition, small intestine goblet cell density was assessed, as mucus production by the goblet cells is important for intestinal integrity. No difference was found in labeling and, consequently, in small intestine goblet cell density between the two phenotypes of mice (B10 mice, 52.1 ± 8.3 cells/mm^2; *mdx* mice, 54.1 ± 4.3 cells/mm^2) (Figure 5, B and C). The intestinal smooth muscle properties were assessed with the *ex vivo* contractility test, and the mean period of spontaneous basal contraction of jejunum was calculated. The period of peristalsis was significantly longer in 1-year−old *mdx* mice than in B10 littermates, suggesting a slowing of peristalsis ($P < 0.01$) (Figure 5D).

Reduction of Ileum Gene Expressions Linked with Intestinal Functionality/Permeability in *mdx* Genotype

Analysis of the expression in ileum samples of various genes linked to intestinal functionality/permeability showed that *Zo-1* and *Zo-2* were significantly down-regulated in *mdx* mice compared with B10 mice ($P < 0.05$) (Figure 6, A and B). Similarly, the gene encoding the SCFA receptor *Ffar2* was down-regulated in *mdx* mice ($P < 0.05$) (Figure 6C). Conversely, *Angptl4* was up-regulated in *mdx* mice ($P < 0.005$) (Figure 6D). Expression of genes encoding inflammatory markers, amino acid receptors, and lipid transporters were comparable between genotypes (data not shown).

Dysregulation of Muscle-Specific Receptors of Gut Bacterial Metabolites and Activation of the Muscle *Tlr4/MyD88* Pathway in *mdx* Genotype

In TA samples, gene expression of *Bcat2* (the skeletal muscle−specific isoform of transaminase 2) was strongly up-regulated in *mdx* mice compared with B10 mice at both ages (Figure 7A). In contrast, in oxidative soleus muscle, *Bcat2* expression was down-regulated at both ages in *mdx* mice (12 weeks, 0.42 ± 0.2-fold change versus B10 mice; 1 year, 0.56 ± 0.07-fold change versus B10 mice; $P < 0.01$).

The adiponectin receptor 1 expression was also up-regulated at both ages in *mdx* TA muscle (Figure 7B), whereas the nonmuscle-specific adiponectin receptor 2 was not significantly different (Figure 7C). Interestingly, in soleus muscle, *adipor1* (12 weeks, 0.73 ± 0.16-fold change versus B10 mice; 1 year, 0.79 ± 0.08-fold change versus B10 mice; $P < 0.01$) and *adipor2* (12 weeks, 0.64 ± 0.19-fold change versus B10 mice; 1 year, 0.76 ± 0.06-fold change versus B10 mice; $P < 0.001$) were significantly down-regulated in *mdx* mice compared with B10 mice from 12 weeks old to 1 year old.

FLA 5.6.0 DTD ■ AJPA3994_proof ■ 24 November 2023 ■ 1:30 am ■ EO: AJPA-D-22-

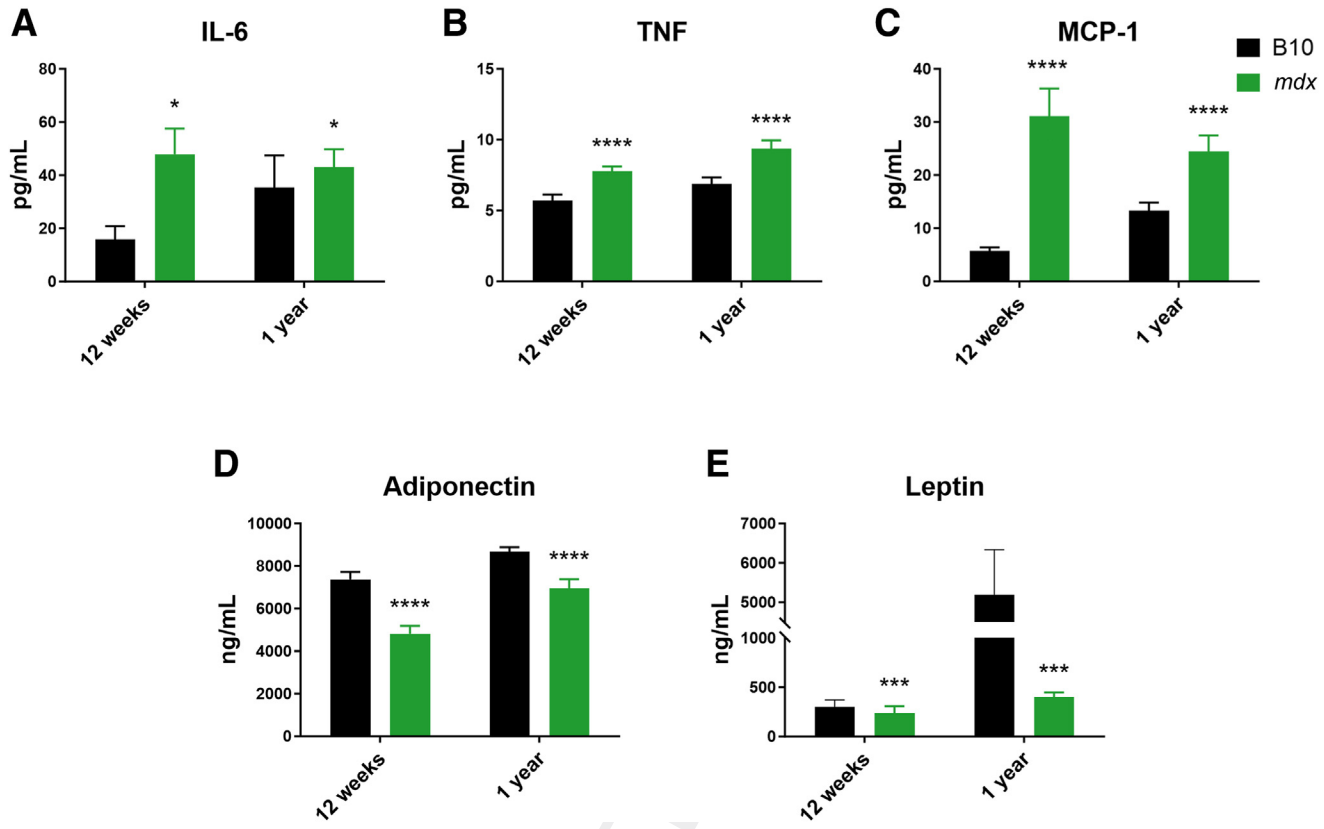

Figure 4 *mdx*-Specific plasma profile associated with gut microbiota signature. **A**–**E:** Levels of IL-6 (**A**), tumor necrosis factor (TNF) (**B**), monocyte chemoattractant protein-1 (MCP-1) (**C**), adiponectin (**D**), and leptin (**E**) in *mdx* (C57BL10SnSc-DMD^{mdx}/J) mice compared with B10 (wild-type C57BL10SnSc) mice at 12 weeks and 1 year of age. $n = 10$ per group per age. *$P < 0.05$, ***$P < 0.001$, ****$P < 0.0001$ versus B10 mice.

The mRNA level of *Tlr4/Myd88* inflammation pathway showed a high activation in *mdx* mice muscles compared with those of B10 mice (Figure 8). The expression of the gene encoding the Toll-like receptor 4, which recognizes pathogen-associated molecular patterns and specifically bacterial lipopolysaccharides, was up-regulated in TA at both ages (Figure 8A) and soleus at 1 year old (B10 mice, 0.68 ± 0.09; *mdx* mice, 1.08 ± 0.08; interaction, $P < 0.001$) in *mdx* mice compared with B10 mice. In *mdx* mice, *Myd88* also was significantly up-regulated in TA (Figure 8B) and soleus (12 weeks, 1.60 ± 0.9-fold change versus B10 mice; 1 year, 1.05 ± 0.2-fold change versus B10 mice; $P = 0.02$) muscles. *Angptl4*, known to be up-regulated during inflammation, was highly up-regulated only in TA muscle (Figure 8C). The expression of other genes linked to gut microbiota metabolites (Table 1) was not different between genotypes (data not shown).

Table 2 Plasma Biomarkers and Their Effect on Gut Microbiota Signature

Marker	Sum of squares	R^2	Statistic	P
TNF (pg/mL)	0.2268	0.1328	2.144	**0.006200**
Leptin (pg/mL)	0.2041	0.1195	1.901	**0.01830**
Adiponectin (ng/mL)	0.1825	0.1069	1.675	**0.04720**
MCP-1 (pg/mL)	0.1823	0.1068	1.673	**0.03700**
Ghrelin active (pg/mL)	0.1253	0.1659	1.193	0.2032
IL-4 (pg/mL)	0.07851	0.1219	0.6944	0.7855
PYY (pg/mL)	0.1624	0.09510	1.471	0.08810
GLP-1 active (pM)	0.1494	0.08752	1.343	0.1066
IL-1β (pg/mL)	0.1155	0.08642	1.041	0.3317
GLP-1 Total (pM)	0.1428	0.08362	1.278	0.1726
IL-6 (pg/mL)	0.1345	0.07876	1.197	0.2147

GLP-1, glucagon-like peptide-1; MCP-1, monocyte chemoattractant protein-1; PYY, peptide YY; TNF, tumor necrosis factor.
Bold: $P < 0.05$.

Discussion

This is the first study designed to explore gut microbiota in *mdx* mice to investigate the gut microbiota–skeletal muscle crosstalk. Monitoring *mdx* mice and B10 wild-type littermates at 8 weeks, 12 weeks, 6 months, and 1 year of age highlighted a unique intestinal bacterial composition in *mdx* mice associated with an impairment of specific plasma and muscle inflammatory biomarker levels. We also confirmed a slowing of gut peristalsis independently of dystrophin deficiency in smooth muscle combined with the intestinal structure impairment in *mdx* mice. Taken together, these alterations might contribute to

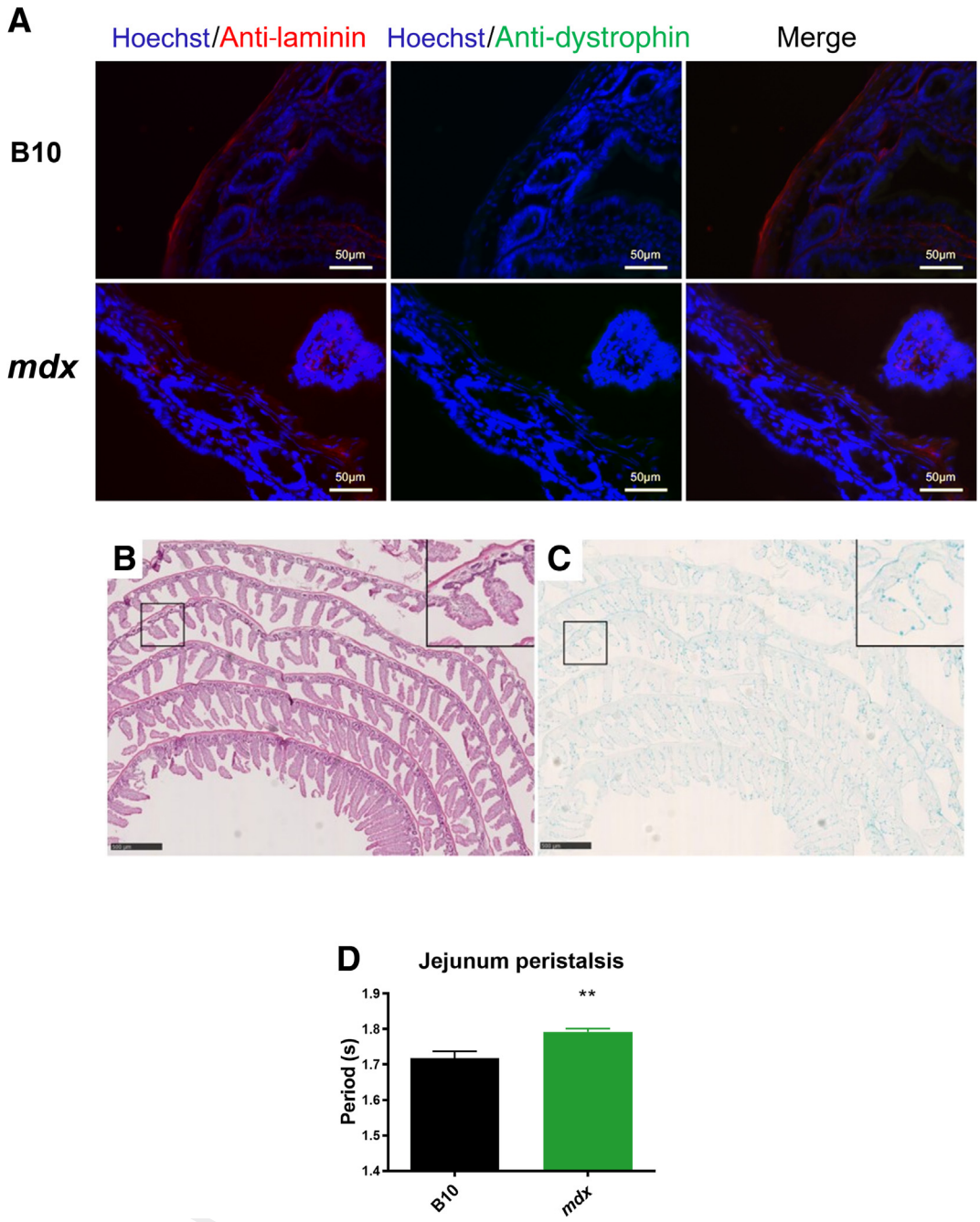

Figure 5 Gut peristalsis and villi structure are impaired in 1-year–old mice independently of dystrophin expression. **A:** Ileum staining with anti-laminin, anti-dystrophin, and Hoechst at 1 year old for both genotypes. **B:** General morphology of villi intestine in Swiss Roll. Sections were stained with hematoxylin and eosin (**B**) and Alcian blue (**C**) in 1-year–old B10 (wild-type C57BL10SnSc) mice. **D:** Jejunum peristalsis at 1 year of age in *mdx* (C57BL10SnSc-DMD^{mdx}/J) mice compared with B10 mice. $n = 8$ per group (**A**); $n = 5$ per group (**B** and **C**); $n = 10$ per group. $^{**}P < 0.01$ versus B10 mice. Scale bars: 50 µm (**A**); 500 µm (**B** and **C**). Magnified boxed area: ×20 (**B** and **C**).

worsen the physiopathology of the skeletal muscle in *mdx* mice.

Q21 The impact of dystrophin deficiency on gut microbiota host. The lower Observed and Chao1 indices in *mdx* mice revealed reduced richness, and the increased InvSimpson index highlighted fewer dominant species and greater evenness. Thus, in *mdx* mice, the overall number of different OTUs and their abundance were significantly reduced. The nonsignificant difference of the Shannon index suggests that this overall lower diversity does not concern rare OTUs. Principal coordinates analysis plots for β-diversity clearly clustered the two genotypes, independently of age. Indeed, *mdx* genotype predicted 20% of β-diversity divergence, validating the theory that dystrophin deficiency affects bacterial composition from birth.

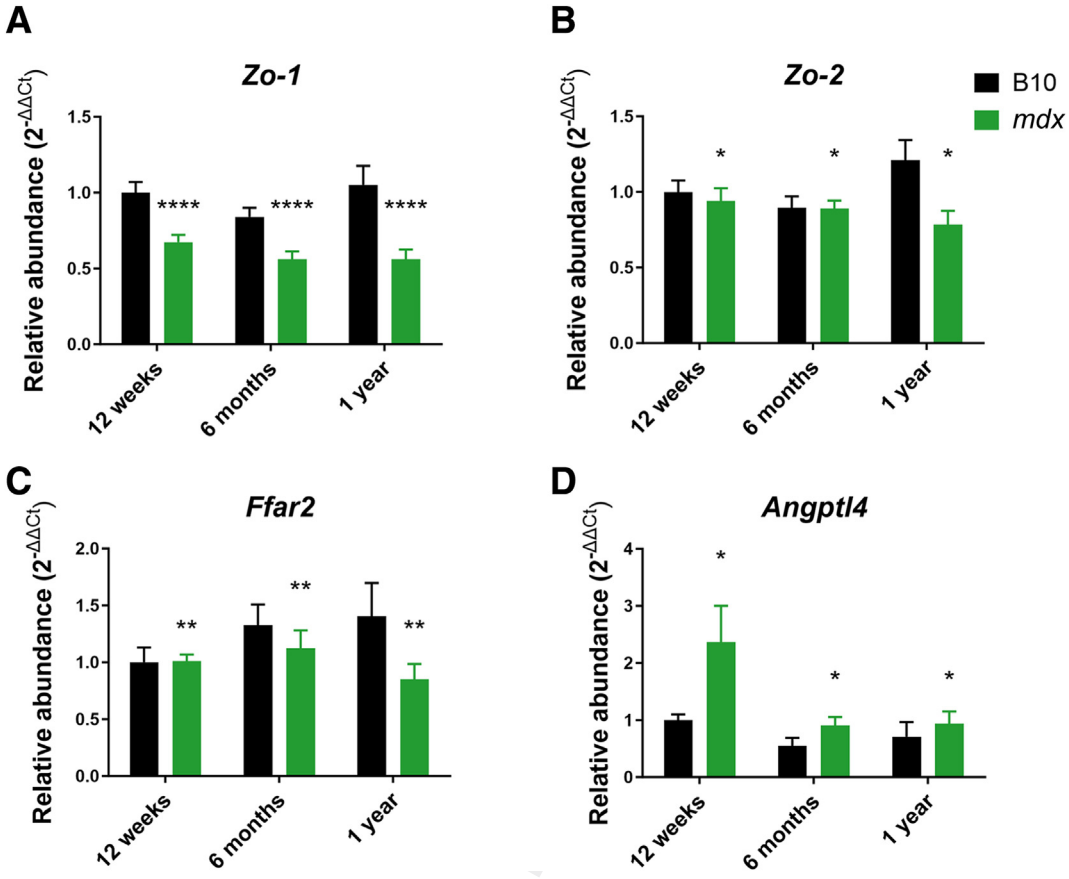

Figure 6 In *mdx* (C57BL10SnSc-DMD^{mdx}/J) mice, alteration of gut microbiota composition is associated with gene expression dysregulation in ileum. **A:** *Zo-1* (zonula occludens 1). **B:** *Zo-2* (zonula occludens 2). **C:** *Ffar2* (free-fatty acid receptor 2). **D:** *Angptl4* (fasting-induced adipose factor). $n = 8$ per group per age. *$P < 0.05$, **$P < 0.01$, ****$P < 0.0001$ versus B10 (wild-type C57BL10SnSc) mice.

Besides the gut microbiota diversity, the metagenomic analysis revealed strong taxonomic modifications. The abundances of four main phyla (Actinobacteria, Proteobacteria, Tenericutes, and Deferribacteres) were increased in *mdx* mice. For three of them, this concerned the phyla and also the included genera (LEfSe analysis): the *Mucispirillum* genus and *Deferribacteraceae* family in the Deferribacteres phylum; the *Enterorhabdus* genus and *Coriobacteriaceae* family in the Actinobacteria phylum; and the *Rhodospirillaceae* family in the Proteobacteria phylum were the most concerned. Interestingly, the Deferribacteres phylum and related taxa were only detected in stools from *mdx* mice and

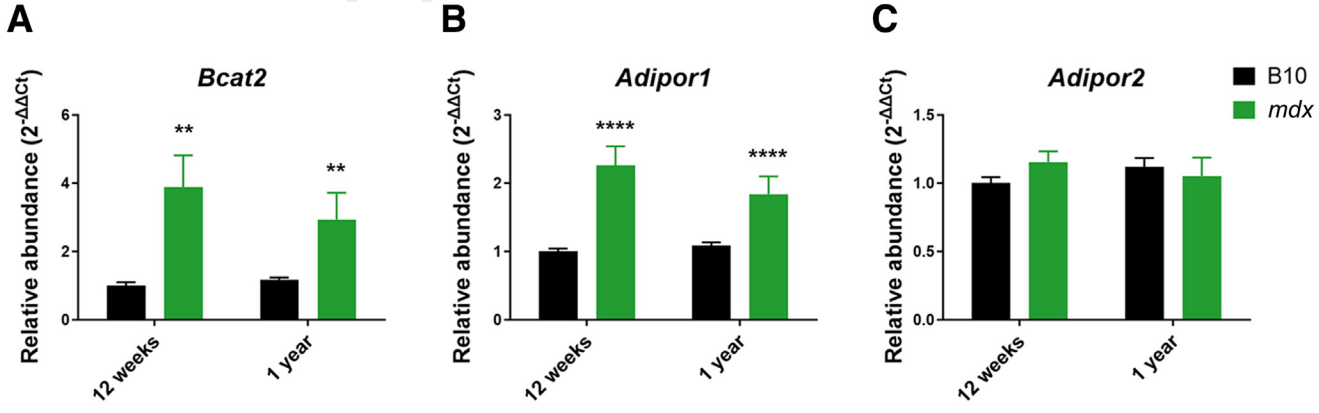

Figure 7 The gene expressions of receptors linked to gut microbiota metabolites are modulated in tibial anterior muscle of *mdx* (C57BL10SnSc-DMD^{mdx}/J) mice. **A:** *Bcat2* (branch-chained amino acids transporter 2). **B:** *Adipor1* (adiponectin receptor 1). **C:** *Adipor2* (adiponectin receptor 2). $n = 8$ per group per age. **$P < 0.01$, ****$P < 0.0001$ versus B10 (wild-type C57BL10SnSc) mice.

FLA 5.6.0 DTD ■ AJPA3994_proof ■ 24 November 2023 ■ 1:30 am ■ EO: AJPA-D-22-

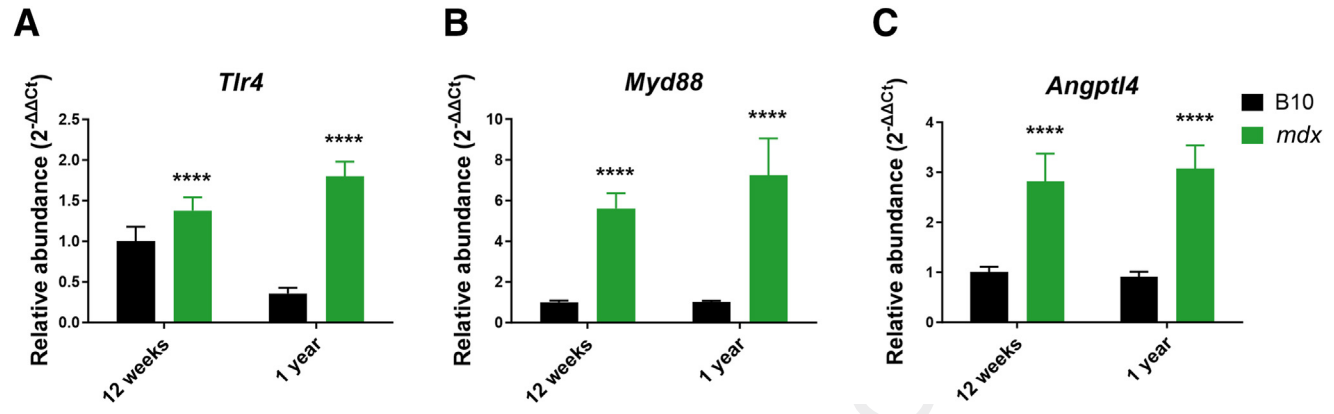

Figure 8 Up-regulation of the skeletal muscle inflammation *Tlr4/Myd88* pathway in tibial anterior muscle of *mdx* (C57BL10SnSc-DMD^{mdx}/J) mice. **A:** *Tlr4* (Toll-like receptor 4). **B:** *Myd88* (myeloid differentiation primary response 88). **C:** *Angptl4* (fasting induce adipose factor). $n = 8$ per group per age. ****$P < 0.0001$ versus B10 (wild-type C57BL10SnSc) mice .

not in wild-type littermates, thus constituting a specific phylum and taxa related to dystrophin deficiency. This phylum includes six genera that are all Gram-negative bacteria.[42]

To the best of our knowledge, these are original results, and no similar data have been published previously on this DMD model. Nevertheless, some hypotheses on the potential links between these microbiota abundance modifications and the dystrophic phenotype could be proposed based on findings of other pathologic models. For instance, in a mouse model of colorectal cancer, an increase in *Mucispirillum schaedleri* drives lipopolysaccharide production that is associated with an inflammatory response.[43] In a model of ulcerative colitis (inflammatory bowel disease family), the active period of the disease is characterized by a larger abundance of Rhodospirillales.[44] Clostridial are in close relationship with intestinal cells, to possibly modulating gut cells' immune processes.[45] Some Enterorhabdus-related species are known to degrade mucus and could expose the intestinal barrier to assault.[46] The combination of metagenomic and metatranscriptomic analyses might reveal the functional activity and implication in the dystrophic phenotype development of the specific commensal microbes identified in the current study.

The current study also found that in *mdx* mice, gut microbiota composition changes were associated with slowed intestinal motility, emphasized by the increased jejunum basal contraction wave period. This result is in accordance with a recent study by Singh et al[47] showing fewer full peristaltic waves in *mdx* mice associated with reduced contraction-stimulated force and mRNA expression of contractile proteins. Furthermore, dystrophin protein was not revealed by intestine staining, either in the control B10 group or in the *mdx* mice. Thus, the difference of intestinal microbiota between *mdx* and B10 is unlikely due to the absence of the dystrophin protein. In addition, the down-regulation of genes encoding the tight junction proteins (*Zo-1* and *Zo-2*), crucial for the epithelial barrier integrity maintenance[48,49] observed in *mdx* ileum samples, indicates a potential impact on the epithelial barrier permeability. Furthermore, results on the gut microbiota suggest that intestine bacteria could play a role in the intestinal dysfunction observed in *mdx* mice. The unique gut microbiota signature Q22 in *mdx* mice with the over-representation of Gram-negative bacteria could promote inflammation in the lumen and disrupt the intestinal contractile properties, comforting the hypothesis of the low-grade circulating inflammation (discussed later). Moreover, *Ffar2* (SCFA receptor) down-regulation in *mdx* ileum highlights lower SCFA production that could alter the smooth muscle metabolism and contractile function.[50–52] Interestingly, *Bcat2* profiles suggest a modulation of bioavailability of branched-chain amino acids. Because branched-chain amino acid production is partially regulated by the gut microbiota, the alteration of the gut microbiota in *mdx* mice could contribute to impairment in this production. Nevertheless, *Bcat2* up-regulation in TA and the opposite down-regulation in soleus indicate a more complicated and intricate response between muscle phenotypes, warranting further investigations.

The reduced *Zo-1* and *Zo-2* expression suggest an increased gut permeability that might lead to a leak of bacterial components in the circulatory system, thus contributing to low-grade inflammation, as confirmed by higher plasmatic levels of IL-6, tumor necrosis factor, and MCP-1 observed in *mdx* mice and/or bacterial infections in distant organs.[53] Furthermore, the LEfSe analysis showed an increase in lipopolysaccharide-producing Gram-negative bacteria (Deferribacteres phylum, *Bacteroides* genus) in *mdx* mice gut. Concomitantly, the gene expression of *Tlr4* (receptor of lipopolysaccharide), *myd88*, and *Angptl4* important proteins of the inflammation pathway were up-regulated in skeletal muscles of *mdx* mice, especially in the tibial anterior. Thus, alteration of gut microbiota associated with disruption of the intestinal barrier could worsen inflammation in dystrophin-deficient skeletal muscle. Finally, circulating adipokine

dysregulation such as adiponectin, ghrelin, and leptin may indicate an adipose tissue disruption in *mdx* mice. Interestingly, the expression of *adipor1*, the suspected main driver of adiponectin cascade in skeletal muscle,[54,55] was altered in TA and soleus muscles from *mdx* mice (TA, up-regulation; soleus, down-regulation). The various patterns highlighted in mixed TA and oxidative soleus muscles might be explained by a different metabolism associated with the typology. Indeed, adiponectin electrophoresis in skeletal muscle has been shown to modulate myosin heavy chain genes toward oxidative phenotype.[56] Thus, adiponectin stimulation might be linked to muscle typology. Interestingly, plasma biomarker analysis also revealed a massive release of leptin in the blood flow at 1 year of age in B10 mice compared with *mdx* mice. Although this satiety hormone has not been studied intensively in the dystrophin-deficiency field, a lower level of leptin could be explained by the *mdx* fat metabolism impairment.[57] These findings raise questions on a third contributor as adipose tissue in the interorgan crosstalk.

To summarize, this original article observed for 1 year the gut microbiota signature in relation with the intestinal structure and function as well as blood biomarkers and skeletal muscle function in a context of dystrophin deficiency. These results showed a strong gut microbiota clustering between genotype, independently of age, with a modulation of four main phyla and genera related to inflammation with overall less diversity in *mdx* mice. Twenty percent of the β-diversity divergence was explained by the genotype, confirming the relationship between dystrophin deficiency and gut bacterial composition from birth. An over-representation of lipopolysaccharide-producing Gram-negative bacteria is shown in *mdx* mice, with reduced intestinal motility as well as gene expressions of ileum tight junction proteins, which suggest an increased intestinal porosity contributing to the low-grade inflammation. This is supported by the systemic inflammation, the up-regulation of bacterial pro-inflammatory receptor *Tlr4/Myd88* in *mdx* muscles, and the adipose tissue secretion profile. Finally, the decrease of *Ffar2* in the ileum might reveal a dysregulation of the gut microbiota SCFA production and bioavailability for skeletal muscles. This study highlights gut microbiota as a potential central metabolic organ in *mdx* physiopathology.[58] Additional studies would be required to better understand gut microbiota involvement in dystrophy development/progression through the intestine−skeletal muscle crosstalk. This finding also encourages studies to develop novel approaches to address the gastrointestinal and muscle dysfunction in patients with DMD to improve the global therapeutic management of muscular dystrophies.

Acknowledgments

We thank the INRAE MIGALE bioinformatics facility (MIGALE, INRAE, 2020; Migale bioinformatics Facility, Jouy-en-Josas, France) for providing and storage resources. We thank Veronique Douard for her gift of phyla primers. We also thank the animal staff from the METAMUS DMEM platform facility, which belongs to the Montpellier Animal Facilities Network, as well as Pierre Delobel for his coding script regarding contractile properties files. We acknowledge the imaging facility MRI, member of the national infrastructure France-BioImaging infrastructure supported by the French National Research Agency (ANR-10-INBS-04, "Investments for the Future"). The authors thank Elisabetta Andermarcher for expert manuscript editing.

Author Contributions

M.J., B.G., A.B, V.O., and C.K.-R. conceptualized the study; M.J, M.M, L.P, O.R, V.O, S.R, B.V, C.B.-G., B.G., and C.K.-R. developed methodology; M.J., B.G., M.M., O.R., S.R., B.G., and C.K.-R. performed software analysis; C.B.-G., M.M., V.O., A.B., B.G., and C.K.-R. validated data; M.J., B.G., V.O., M.M., O.R., L.P., C.B-G., A.B., B.G., and C.K.-R. analyzed data; M.J., B.G., L.P., V.O., A.B., and C.K.-R. performed investigations; B.G., V.O., A.B., and C.K.-R. provided resources; M.J., O.R., M.M., L.P., B.G., and C.K.-R. curated data; M.J., B.G., and C.K.-R. wrote the manuscript; M.J., M.M., O.R., V.O., A.B., S.R., C.B.-G., V.O., B.G., and C.K.-R. reviewed and edited the manuscript; M.J., B.G., V.O., and C.K.-R. visualized data; B.G. and C.K.-R. supervised the study; and V.O., B.G., and C.K.-R. administered the project. All authors have read and agreed to the published version of the manuscript.

Disclosure Statement

None declared. The funders had no role in the design of the study; in the collection, analyses, or interpretation of data; in the writing of the manuscript; or in the decision to publish the results.

Supplemental Data

Supplemental material for this article can be found at *http://doi.org/10.1016/j.ajpath.2023.10.010*.

References

1. Porter JD, Khanna S, Kaminski HJ, Rao JS, Merriam AP, Richmonds CR, Leahy P, Li J, Guo W, Andrade FH: A chronic inflammatory response dominates the skeletal muscle molecular signature in dystrophin-deficient mdx mice. Hum Mol Genet 2002, 11:263−272
2. Rosenberg AS, Puig M, Nagaraju K, Hoffman EP, Villalta SA, Rao VA, Wakefield LM, Woodcock J: Immune-mediated pathology in Duchenne muscular dystrophy. Sci Transl Med 2015, 7:299rv4
3. Fong PY, Turner PR, Denetclaw WF, Steinhardt RA: Increased activity of calcium leak channels in myotubes of Duchenne human and mdx mouse origin. Science 1990, 250:673−676

4. Gailly P: New aspects of calcium signaling in skeletal muscle cells: implications in Duchenne muscular dystrophy. Biochim Biophys Acta 2002, 1600:38–44
5. Rando TA, Disatnik MH, Yu Y, Franco A: Muscle cells from mdx mice have an increased susceptibility to oxidative stress. Neuromuscul Disord 1998, 8:14–21
6. Pauly M, Daussin F, Burelle Y, Li T, Godin R, Fauconnier J, Koechlin-Ramonatxo C, Hugon G, Lacampagne A, Coisy-Quivy M, Liang F, Hussain S, Matecki S, Petrof BJ: AMPK activation stimulates autophagy and ameliorates muscular dystrophy in the mdx mouse diaphragm. Am J Pathol 2012, 181:583–592
7. Kuznetsov AV, Winkler K, Wiedemann FR, von Bossanyi P, Dietzmann K, Kunz WS: Impaired mitochondrial oxidative phosphorylation in skeletal muscle of the dystrophin-deficient mdx mouse. Mol Cell Biochem 1998, 183:87–96
8. Vila MC, Rayavarapu S, Hogarth MW, Van der Meulen JH, Horn A, Defour A, Takeda S, Brown KJ, Hathout Y, Nagaraju K, Jaiswal JK: Mitochondria mediate cell membrane repair and contribute to Duchenne muscular dystrophy. Cell Death Differ 2017, 24:330–342
9. Verhaart IEC, Aartsma-Rus A: Therapeutic developments for Duchenne muscular dystrophy. Nat Rev Neurol 2019, 15:373–386
10. Sheikh O, Yokota T: Developing DMD therapeutics: a review of the effectiveness of small molecules, stop-codon readthrough, dystrophin gene replacement, and exon-skipping therapies. Expert Opin Investig Drugs 2021, 30:167–176
11. Hyzewicz J, Ruegg UT, Takeda S: Comparison of experimental protocols of physical exercise for mdx mice and Duchenne muscular dystrophy patients. J Neuromuscul Dis 2015, 2:325–342
12. Radley HG, De Luca A, Lynch GS, Grounds MD: Duchenne muscular dystrophy: focus on pharmaceutical and nutritional interventions. Int J Biochem Cell Biol 2007, 39:469–477
13. Viaud S, Saccheri F, Mignot G, Yamazaki T, Daillère R, Hannani D, Enot DP, Pfirschke C, Engblom C, Pittet MJ, Schlitzer A, Ginhoux F, Apetoh L, Chachaty E, Woerther P-L, Eberl G, Bérard M, Ecobichon C, Clermont D, Bizet C, Gaboriau-Routhiau V, Cerf-Bensussan N, Opolon P, Yessaad N, Vivier E, Ryffel B, Elson CO, Doré J, Kroemer G, Lepage P, Boneca IG, Ghiringhelli F, Zitvogel L: The intestinal microbiota modulates the anticancer immune effects of cyclophosphamide. Science 2013, 342:971–976
14. Iida N, Dzutsev A, Stewart CA, Smith L, Bouladoux N, Weingarten RA, Molina DA, Salcedo R, Back T, Cramer S, Dai R-M, Kiu H, Cardone M, Naik S, Patri AK, Wang E, Marincola FM, Frank KM, Belkaid Y, Trinchieri G, Goldszmid RS: Commensal bacteria control cancer response to therapy by modulating the tumor microenvironment. Science 2013, 342:967–970
15. Alexander JL, Wilson ID, Teare J, Marchesi JR, Nicholson JK, Kinross JM: Gut microbiota modulation of chemotherapy efficacy and toxicity. Nat Rev Gastroenterol Hepatol 2017, 14:356–365
16. Bindels LB, Beck R, Schakman O, Martin JC, De Backer F, Sohet FM, Dewulf EM, Pachikian BD, Neyrinck AM, Thissen J-P, Verrax J, Calderon PB, Pot B, Grangette C, Cani PD, Scott KP, Delzenne NM: Restoring specific lactobacilli levels decreases inflammation and muscle atrophy markers in an acute leukemia mouse model. PloS One 2012, 7:e37971
17. Hsu YJ, Chiu CC, Li YP, Huang WC, Huang YT, Huang CC, Chuang HL: Effect of intestinal microbiota on exercise performance in mice. J Strength Cond Res 2015, 29:552–558
18. Tung Y-T, Chen Y-J, Chuang H-L, Huang W-C, Lo C-T, Liao C-C, Huang C-C: Characterization of the serum and liver proteomes in gut-microbiota-lacking mice. Int J Med Sci 2017, 14:257–267
19. Nay K, Jollet M, Goustard B, Baati N, Vernus B, Pontones M, Lefeuvre-Orfila L, Bendavid C, Rué O, Mariadassou M, Bonnieu A, Ollendorff V, Lepage P, Derbre F, Koechlin-Ramonatxo C: Gut bacteria are critical for optimal muscle function: a potential link with glucose homeostasis. Am J Physiol Endocrinol Metab 2019, 317:E158–E171
20. Yan H, Diao H, Xiao Y, Li W, Yu B, He J, Yu J, Zheng P, Mao X, Luo Y, Zeng B, Wei H, Chen D: Gut microbiota can transfer fiber characteristics and lipid metabolic profiles of skeletal muscle from pigs to germ-free mice. Sci Rep 2016, 6:31786
21. Gao Z, Yin J, Zhang J, Ward RE, Martin RJ, Lefevre M, Cefalu WT, Ye J: Butyrate improves insulin sensitivity and increases energy expenditure in mice. Diabetes 2009, 58:1509–1517
22. Vannucchi M-G, Zardo C, Corsani L, Faussone-Pellegrini M-S: Interstitial cells of Cajal, enteric neurons, and smooth muscle and myoid cells of the murine gastrointestinal tract express full-length dystrophin. Histochem Cell Biol 2002, 118:449–457
23. Boland B, Himpens B, Denef JF, Gillis JM: Site-dependent pathological differences in smooth muscles and skeletal muscles of the adult mdx mouse. Muscle Nerve 1995, 18:649–657
24. Lo Cascio CM, Goetze O, Latshang TD, Bluemel S, Frauenfelder T, Bloch KE: Gastrointestinal dysfunction in patients with Duchenne muscular dystrophy. PloS One 2016, 11:e0163779
25. Cerdá B, Pérez M, Pérez-Santiago JD, Tornero-Aguilera JF, González-Soltero R, Larrosa M: Gut microbiota modification: another piece in the puzzle of the benefits of physical exercise in health? Front Physiol 2016, 7:51
26. Mangera Z, Panesar G, Makker H: Practical approach to management of respiratory complications in neurological disorders. Int J Gen Med 2012, 5:255–263
27. Baccari MC, Nistri S, Vannucchi MG, Calamai F, Bani D: Reversal by relaxin of altered ileal spontaneous contractions in dystrophic (mdx) mice through a nitric oxide-mediated mechanism. Am J Physiol Regul Integr Comp Physiol 2007, 293:R662–R668
28. Mulè F, Amato A, Serio R: Gastric emptying, small intestinal transit and fecal output in dystrophic (mdx) mice. J Physiol Sci 2010, 60:75–79
29. Swiderski K, Bindon R, Trieu J, Naim T, Schokman S, Swaminathan M, Leembruggen AJL, Hill-Yardin EL, Koopman R, Bornstein JC, Lynch GS: Spatiotemporal mapping reveals regional gastrointestinal dysfunction in mdx dystrophic mice ameliorated by oral L-arginine supplementation. J Neurogastroenterol Motil 2020, 26:133–146
30. Mancinelli R, Tonali P, Servidei S, Azzena GB: Analysis of peristaltic reflex in young mdx dystrophic mice. Neurosci Lett 1995, 192:57–60
31. Tameyasu T, Ogura S, Ogihara K: The effect of e-, i-, and n-nitric oxide synthase inhibition on colonic motility in normal and muscular dystrophy (mdx) mice. Jpn J Physiol 2004, 54:555–566
32. Ploquin C, Chabi B, Fouret G, Vernus B, Feillet-Coudray C, Coudray C, Bonnieu A, Ramonatxo C: Lack of myostatin alters intermyofibrillar mitochondria activity, unbalances redox status, and impairs tolerance to chronic repetitive contractions in muscle. Am J Physiol Endocrinol Metab 2012, 302:E1000–E1008
33. Alves GA, Silva LR, Rosa EF, Aboulafia J, Freymüller-Haapalainen E, Souccar C, Nouailhetas VL: Intestine of dystrophic mice presents enhanced contractile resistance to stretching despite morphological impairment. Am J Physiol Gastrointest Liver Physiol 2014, 306:G191–G199
34. Pereira ESA, Lourenco AL, Marmello BO, Bitteti M, Teixeira G: Comparison of two techniques for a comprehensive gut histopathological analysis: Swiss Roll versus intestine strips. Exp Mol Pathol 2019, 111:104302
35. Mariat D, Firmesse O, Levenez F, Guimarães V, Sokol H, Doré J, Corthier G, Furet J-P: The Firmicutes/Bacteroidetes ratio of the human microbiota changes with age. BMC Microbiol 2009, 9:123
36. Escudié F, Auer L, Bernard M, Mariadassou M, Cauquil L, Vidal K, Maman S, Hernandez-Raquet G, Combes S, Pascal G: FROGS: find, rapidly, OTUs with Galaxy Solution. Bioinformatics 2018, 34:1287–1294
37. Bernard M, Rué O, Mariadassou M, Pascal G: FROGS: a powerful tool to analyse the diversity of fungi with special management of internal transcribed spacers. Brief Bioinform 2021, 22:bbab318

38. Quast C, Pruesse E, Yilmaz P, Gerken J, Schweer T, Yarza P, Peplies J, Glöckner FO: The SILVA ribosomal RNA gene database project: improved data processing and web-based tools. Nucleic Acids Res 2013, 41:D590−D596
39. McMurdie PJ, Holmes S: phyloseq: an R package for reproducible interactive analysis and graphics of microbiome census data. PloS One 2013, 8:e61217
Q26 40. Wickham H: ggplot2. Elegant Graphics For Data Analysis, 2009
41. Segata N, Izard J, Waldron L, Gevers D, Miropolsky L, Garrett WS, Huttenhower C: Metagenomic biomarker discovery and explanation. Genome Biol 2011, 12:R60
42. Alauzet C, Jumas-Bilak E: The phylum Deferribacteres and the genus Caldithrix. Edited by Rosenberg E, DeLong EF, Lory S,
Q27 Stackebrandt E, Thompson F. In The Prokaryotes; 2014
43. Daniel SG, Ball CL, Besselsen DG, Doetschman T, Hurwitz BL: Functional changes in the gut microbiome contribute to transforming growth factor [beta]-deficient colon cancer. mSystems 2017, 2: e00065−e00117
44. Yang Y, Chen G, Yang Q, Ye J, Cai X, Tsering P, Cheng X, Hu C, Zhang S, Cao P: Gut microbiota drives the attenuation of dextran sulphate sodium-induced colitis by Huangqin decoction. Oncotarget 2017, 8:48863−48874
45. Lopetuso LR, Scaldaferri F, Petito V, Gasbarrini A: Commensal Clostridia: leading players in the maintenance of gut homeostasis. Gut Pathog 2013, 5:23
46. Derrien M, van Passel MW, van de Bovenkamp JH, Schipper RG, de Vos WM, Dekker J: Mucin-bacterial interactions in the human oral cavity and digestive tract. Gut Microbes 2010, 1:254−268
47. Singh K, Randhwa G, Salloum FN, Grider JR, Murthy KS: Decreased smooth muscle function, peristaltic activity, and gastrointestinal transit in dystrophic (mdx) mice. Neurogastroenterol Motil 2021, 33: e13968
48. Fasano A: Zonulin and its regulation of intestinal barrier function: the biological door to inflammation, autoimmunity, and cancer. Physiol Rev 2011, 91:151−175
49. Ulluwishewa D, Anderson RC, McNabb WC, Moughan PJ, Wells JM, Roy NC: Regulation of tight junction permeability by intestinal bacteria and dietary components. J Nutr 2011, 141:769−776
50. Yajima T: Contractile effect of short-chain fatty acids on the isolated colon of the rat. J Physiol 1985, 368:667−678
51. Suply E, de Vries P, Soret R, Cossais F, Neunlist M: Butyrate enemas enhance both cholinergic and nitrergic phenotype of myenteric neurons and neuromuscular transmission in newborn rat colon. Am J Physiol Gastrointest Liver Physiol 2012, 302:G1373−G1380
52. Mitsui R, Ono S, Karaki S, Kuwahara A: Neural and non-neural mediation of propionate-induced contractile responses in the rat distal colon. Neurogastroenterol Motil 2005, 17:585−594
53. Ghosh SS, Wang J, Yannie PJ, Ghosh S: Intestinal barrier dysfunction, LPS translocation, and disease development. J Endocr Soc 2020, 4:bvz039
54. Iwabu M, Yamauchi T, Okada-Iwabu M, Sato K, Nakagawa T, Funata M, Yamaguchi M, Namiki S, Nakayama R, Tabata M, Ogata H, Kubota N, Takamoto I, Hayashi YK, Yamauchi N, Waki H, Fukayama M, Nishino I, Tokuyama K, Ueki K, Oike Y, Ishii S, Hirose K, Shimizu T, Touhara K, Kadowaki T: Adiponectin and AdipoR1 regulate PGC-1alpha and mitochondria by Ca(2+) and AMPK/SIRT1. Nature 2010, 464:1313−1319
55. Krause MP, Liu Y, Vu V, Chan L, Xu A, Riddell MC, Sweeney G, Hawke TJ: Adiponectin is expressed by skeletal muscle fibers and influences muscle phenotype and function. Am J Physiol Cell Physiol 2008, 295:C203−C212
56. Abou-Samra M, Boursereau R, Lecompte S, Noel L, Brichard SM: Potential therapeutic action of adiponectin in Duchenne muscular dystrophy. Am J Pathol 2017, 187:1577−1585
57. Strakova J, Kamdar F, Kulhanek D, Razzoli M, Garry DJ, Ervasti JM, Bartolomucci A, Townsend D: Integrative effects of dystrophin loss on metabolic function of the mdx mouse. Sci Rep 2018, 8:13624
58. Marullo AL, O'Halloran KD: Microbes, metabolites and muscle: is the gut-muscle axis a plausible therapeutic target in Duchenne muscular dystrophy? Exp Physiol 2023, 108:1132−1143